STUDIA UBB CHEMIA, LXX, 3, 2025 (p. 21-33)
(RECOMMENDED CITATION)
DOI:10.24193/subbchem.2025.3.02

MOLYBDENUM FLAT COIL FILAMENT FOR SAMPLE INTRODUCTION AND MULTIELEMENTAL DETERMINATION BY SMALL-SIZED ELECTROTHERMAL VAPORIZATION CAPACITIVELY COUPLED MICROPLASMA OPTICAL EMISSION SPECTROMETRY

Sergiu CADAR[a], Adrian-Ioan DUDU[b,c], Dorin PETREUS[d], Simion Bogdan ANGYUS[a], Maria FRENTIU[a], Eniko COVACI[b,e,*]

ABSTRACT. A novel small-sized electrothermal vaporization device including a molybdenum flat coil filament was studied for sample introduction into a capacitively coupled microplasma (SSETV-μCCP-OES) for the simultaneous multielemental determination of Cu, Zn, Pb, Cd, Hg, Se, Te, Sb and Bi by optical emission spectrometry. The limits of detection, obtained by this experimental setup were 2–25 times lower than those previously obtained using a Rh coil filament, ranging from 0.16 μg L^{-1} for Cd to 10.7 μg L^{-1} for Se. This improvement was primarily attributed to the more efficient heating of the Mo flat coil filament compared to the Rh coil filament, considering that Rh has a lower melting point and therefore must be heated more gradually. Consequently, in the transient spectra recorded using the Mo flat coil filament the maximum signal intensities were observed earlier, ranging from 1.5 s for Hg to 3.3 s for Zn, compared to those obtained with the Rh coil filament, which

[a] *National Institute for Research and Development of Optoelectronics INOE 2000 INCD Bucharest, Research Institute for Analytical Instrumentation, Donath 67, 400293 Cluj-Napoca, Romania.*
[b] *Babeş-Bolyai University, Faculty of Chemistry and Chemical Engineering, 11 Arany Janos str., RO-400028, Cluj-Napoca, Romania.*
[c] *Enzymology and Applied Biocatalysis Research Center, Arany Janos 11, 400028 Cluj-Napoca, Romania.*
[d] *Technical University of Cluj-Napoca, Faculty of Electronics, Telecommunications and Information Technology, Gheorghe Baritiu 26-28, 400027 Cluj-Napoca, Romania.*
[e] *Babeş-Bolyai University, Research Center for Advanced Analysis, Instrumentation and Chemometrics, Arany Janos 11, 400028 Cluj-Napoca, Romania.*
[*] *Corresponding author: eniko.covaci@ubbcluj.ro*

ranged from 2.4 s for Hg to 5.3 s for Cu. The results demonstrate the strong analytical potential of the SSETV device with the Mo flat coil filament, for the simultaneous multielemental trace metal analysis.

Keywords: *electrothermal vaporization, molybdenum flat coil filament, capacitively coupled microsplasma optical emission spectrometry.*

INTRODUCTION

The development of innovative analytical techniques is increasingly steered by the principles of Green Analytical Chemistry, with emphasis on miniaturization and improved sensitivity [1-4]. This approach is closely aligned with lab-on-a-chip paradigms and responds to the growing demand for portable, field-deployable instrumentation across environmental, clinical, and forensic domains [5]. A central challenge in trace elemental analysis lies in the efficient sample introduction techniques into plasma sources [6]. Conventional pneumatic nebulization techniques are often constrained by low analyte transport efficiency, susceptibility to matrix effects, and limited compatibility with microplasma sources [7].

Electrothermal vaporization (ETV) presents a compelling alternative, offering direct analyte vaporization from electrically heated tubes, boats, or filaments [6, 8]. ETV significantly enhances analyte transport efficiency and facilitates temporal separation of analyte from matrix by selective vaporization, and thereby reducing spectral interferences and improving signal-to-noise ratio [6, 9]. Moreover, ETV requires for analysis only microgram-level sample quantities. Collectively, these attributes position ETV as a highly versatile and efficient sample introduction technique for trace elemental and speciation analysis across a wide range of application areas [9-11].

Common heating substrates are commonly made of metals filaments such as W [12-14], Ta [7, 15], Mo [12], Re [5] and Rh [16, 17], as well as composite systems like rhodium-coated tungsten [18], graphite tubes, and emerging metal–ceramic heaters [19]. Compared to graphite furnace used in atomic absorption spectrometry (AAS), metal filaments offer faster heating, lower-power requirements, and reduced memory effects, especially when coated with modifiers like rhodium to enhance durability [8]. Tungsten is most commonly used due to its high melting point, but is prone to oxidation, and they frequently require the presence of hydrogen [18, 20, 21].

Tungsten-based ETV devices have been integrated with a wide range of spectrometric detection techniques, such as atomic absorption spectrometry (AAS) [22], inductively coupled plasma optical emission spectrometry (ICP-

OES) [23], mass spectrometry (ICP-MS) [13], dielectric barrier discharge optical emission spectrometry (DBD-OES) [12] and atmospheric pressure glow discharge atomic emission spectrometry (APGD-AES) [20] for multielemental determination in environmental, food and biological samples. Rhenium and Ta filaments have been applied in ETV systems coupled with AAS, AES, and atomic fluorescence spectrometry (AFS) for trace metal determination, such as Pb, Cu, Mn, Cd, K, Na and Li [5, 7].

Molybdenum on the other hand, has previously been explored for ETV coupled with AAS, ICP-MS, and more recently with dielectric barrier discharge optical emission spectrometry (DBD-OES) for the determination of Zn, Pb, Ag, Cd, Au, Cu, Mn, Fe, Cr and As in various environmental samples [24, 25]. In these studies, only tubular and wire-based filament geometries were employed, in combination with conventional benchtop instruments. Microplasma based configurations remain largely unexplored, and no prior studies have reported of such filament.

Until now, the capacitively coupled microplasma torch has been coupled with a miniaturized sample introduction system based on electrothermal vaporization from a Rh coil filament. Although rhodium offers several important advantages, such as ease of manual handling, high chemical resistance to oxygen and acids used for sample digestion, and the fact that it does not require the presence of hydrogen in the electrothermal vaporization atmosphere, its relatively low melting point of approximately 1963 °C limits the rate of analyte evaporation, which in turn negatively affects the sensitivity of the analysis [16, 17]. Thus, the aim of this study was to design and characterize a novel Mo flat coil filament as sample introduction device for the simultaneous multielemental determination of Cu, Zn, Pb, Cd, Hg, Se, Te, Sb and Bi by small-sized electrothermal vaporization capacitively coupled microplasma optical emission spectrometry (SSETV-μCCP-OES). Limits of detection (LOD) were evaluated based on signal-to-background ratio and relative standard deviation of the background signal (SBR-RSDB) [26, 27] by comparison with those previously obtained with a Rh coil filament.

RESULTS AND DISCUSSION

Figure 1 and 2 illustrate the novel SSETV sample introduction system with a Mo flat coil filament developed for the simultaneous multielemental determination of Cu, Zn, Pb, Cd, Hg, Se, Te, Sb and Bi by μCCP-OES. The system operates in two sequential stages. In the first stage, the filament is heated in air to 80 °C for 180 s to dry the microsample previously pipetted onto its surface, while in the second stage, the filament is heated in Ar flow to 1500 °C

for 10 s to vaporize the sample and introduce it into the microplasma for excitation. Simultaneously with the vaporization step, the emission signals were recorded using the Maya2000 Pro microspectrometer (Ocean Optics, Dunedin, USA) as 100 episodic spectra with 100 ms integration time. A detailed description of the construction and operation of the SSETV device is provided in the Experimental section.

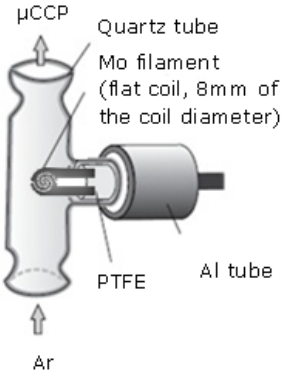

Figure 1. Scheme of the Mo flat coil filament installed in the vaporization chamber

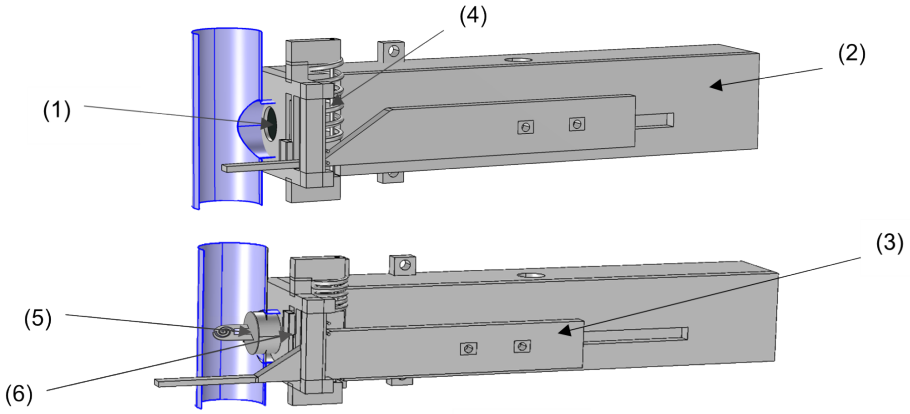

Figure 2. Filament introduction system in sample drying (top) and vaporization (bottom) positions (1 – iris type mechanism; 2 – piston support; 3 – lever; 4 – spring; 5 – Mo flat coil filament fixed on a PTFE piston with the aid of epoxy resin; 6 – iris actuator slider)

An initial study on the excitation capability of the μCCP indicated an optimal operating power of 15 W and an argon consumption rate of 150 mL min^{-1}.

For spectroscopic observation of the plasma, a height of 0.8 mm above the molybdenum tip microelectrode was selected, as previously determined to be optimal for achieving maximum emission signal intensity and enabling simultaneous multielement detection of transient emission spectra [17, 28, 29]. It was also previously observed that a temperature of 1500 °C is sufficient for the evaporation of a significant number of elements from the Rh coil filament, which can be vaporized and excited at resonance lines with excitation energies of up to 7.5 eV [28]. This temperature was also selected for the Mo filament in the present study. A sample volume of 10 µL was employed in all measurements, consistent with those used in previous studies. The optimal operating conditions for the SSETV-µCCP-OES tandem for the simultaneous determination of Cu, Zn, Pb, Cd, Hg, Se, Te, Sb, and Bi using both the Mo flat coil filament and the Rh coil filament are presented in Table 1.

Table 1. The optimal operating conditions of the SSETV-µCCP-OES tandem for the simultaneous determination of Cu, Zn, Pb, Cd, Hg, Se, Te, Sb, and Bi using the Mo flat coil filament and the Rh coil filament

Parameter	**Working conditions**	
	Rh coil filament	**Mo flat coil filament**
Microplasma power	15 W	
Ar flow rate	150 mL min^{-1}	
Observation height	0.8 mm	
Sample drying	80 °C for 180 s (0.25 V, 1.93 A)	80 °C for 180 s (0.1 V, 3.6 A)
Sample vaporization	1500 °C for 10 s (1.62 V, 4.32 A)	1500 °C for 10 s (1.20 V, 12 A)
Spectra registration	100 episodic spectra with 100 ms integration time	

The temperature control of the filaments was verified by optical pyrometry using the Optris 3ML and Optris 1MH1-CF3 IR detectors from Optris GmbH (Berlin, Germany). In contrast to the Rh coil filament, which has a melting point of 1963 °C and needs a current limit of 5 A, the Mo flat coil filament, due to its higher electrical resistance, is characterized by a higher melting point (2620 °C) and can be operated at higher currents of up to 12 A, enabling faster heating. The filament temperature during the vaporization stage was controlled with a precision better than 2% and a bias of +20 °C relative to the target temperature. The power source used for the filaments heating enabled microsecond-level temperature control, resulting in highly reproducible operating temperatures. Under these operating conditions, the evaporation of elements is expected to occur more rapidly with the Mo flat coil filament compared to the Rh coil filament, with a higher instantaneous

analyte flux, resulting in an earlier appearance of the analytical signals and within fewer episodic spectra. Accordingly, based on the higher sensitivity, expressed as signal-to-background ratio (SBR), improved limits of detection are expected to be obtained for the Mo flat coil filament compared to the Rh coil filament.

Figure 3 presents the 3D emission spectra of the elements obtained using the Mo flat coil filament under the optimal operating conditions of the SSETV-μCCP-OES setup.

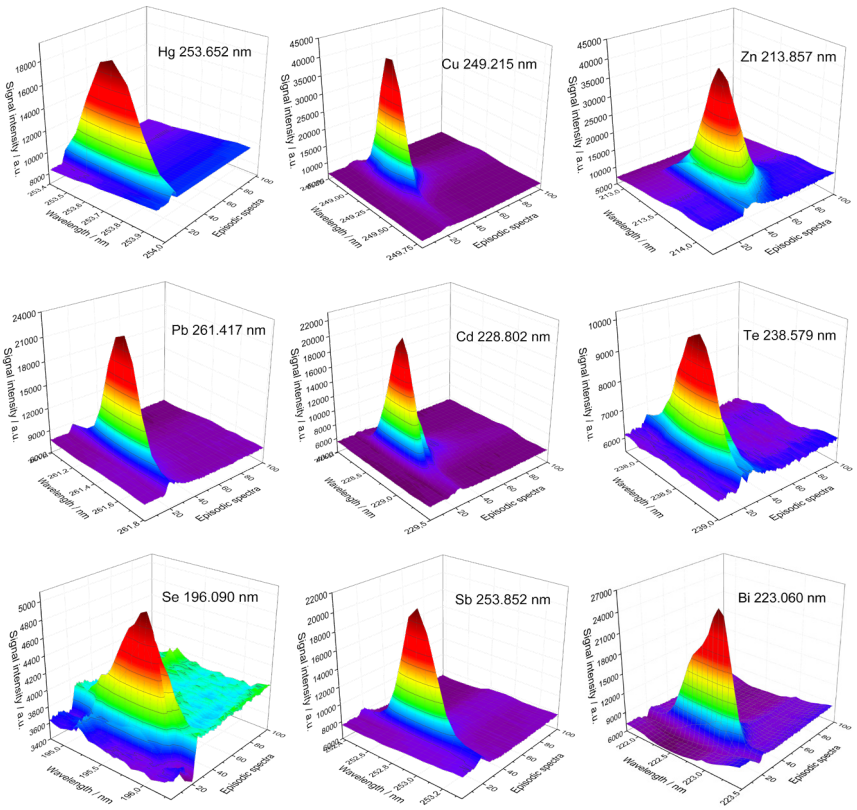

Figure 3. 3D emission spectra (signal intensity, wavelength, time) of Hg, Cu, Zn, Pb, Cd, Te, Se, Sb and Bi recorded by ETV-μCCP-OES using the Mo flat coil filament in measurement conditions: plasma observation height: 0.8 mm above the Mo tip electrode; plasma power: 15 W; Ar flow rate: 150 mL min^{-1}; sample volume: 10 μL; elements concentration: 1 mg L^{-1} Cu, Pb, Te, Se, Sb and Bi and 0.1 mg L^{-1} Cd, Zn and Hg multielement standard solution in 2% (v/v) HNO_3, vaporization: 1500 °C for 10 s

Figure 4 presents the transient net emission signals of elements, along with the times at which maximum signal intensities occurred, obtained by SSETV-μCCP-OES using the Mo flat coil filament under optimized working conditions. It was observed that, except for Zn, all elements reached maximum vaporization between 1.5 s (Hg) and 2.2 s (Cu and Bi). In contrast, previously reported data using a Rh coil filament showed delayed vaporization maxima, with maximum emission signals at 2.4 s Hg; 5.3 s Cu; 4.9 s Zn; 5.2 s Pb; 4 s Te; 3.5 s Se; 4.3 s Sb and 4 s Bi [28, 29]. These findings demonstrate that the Mo flat coil filament provides a more efficient vaporization of the microsample compared to the Rh coil counterpart.

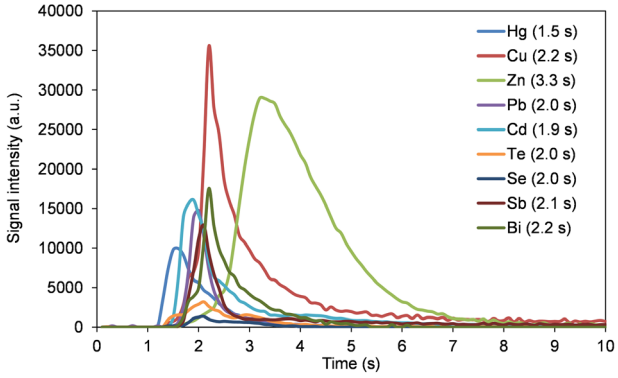

Figure 4. Transient net emission signals of elements at their most sensitive lines recorded by SSETV-μCCP-OES using the Mo flat coil filament in measurement conditions: plasma observation height: 0.8 mm above the Mo tip electrode; sample volume: 10 μL; elements concentration: 1 mg L^{-1} Cu, Pb, Te, Se, Sb and Bi and 0.1 mg L^{-1} Cd, Zn and Hg multielement standard solution in 2% (v/v) HNO_3

The limits of detection obtained using the SBR–RSDB approach [26, 27] for the SSETV-μCCP-OES method, employing both the Mo flat coil and Rh coil filament under optimized working conditions, are presented in Table 2. Signal-to-background ratio values were determined using emission signals recorded using a multielement solution containing 1 mg L^{-1} of Cu, Pb, Te, Se, Sb, and Bi, and 0.1 mg L^{-1} of Cd, Zn, and Hg. Although the concentrations were selected arbitrary, they do not affect the calculated limits of detection, as they fall within the linear dynamic range of the method. Previous work using the same experimental setup with a Rh coiled filament demonstrated linear calibration curves up to concentrations of 5 mg L^{-1}. [28] The RSDB values ranged from 0.5% to 1.5% for the Mo flat coil filament, similar to those obtained with the Rh coil filament, which ranged from 0.8% to 1.9%. Significantly better LODs were achieved using the Mo flat coil filament ranging from 0.16 μg L^{-1} for Cd to 10.7 μg L^{-1} L for Se, compared with the range of 0.28 μg L^{-1} for Cd –

22.6 μg L^{-1} Se for the Rh coil filament. Thus, improvements in the limits of detection (LODs) by factors of 2 to 25 were achieved for the majority of elements, with the exception of copper. This enhancement can be attributed to the faster heating of the Mo flat coil filament, as expected, compared to the Rh filament, which is limited to a current of 5 A, in contrast to 12 A for the Mo filament. A comparison between the LODs obtained by SSETV-μCCP-OES using the Mo flat coil filament and those reported for other microplasma sources equipped with metallic electrothermal vaporization devices used in optical emission spectrometry is presented in Table 3.

Table 2. Analytical figures of merit of the SSETV-μCCP-OES method using the Rh coil and Mo flat coil filaments

Element	λ (nm)[a]	Rh coil filament			Mo flat coil filament		
		RSDB (%)	SBR[b]	LOD[c] (μg L^{-1})	RSDB (%)	SBR[b]	LOD[c] (μg L^{-1})
Hg	253.652	1.1	2.2	1.50	1.2	18.0	0.20
Cu	249.215	1.0	5.0	0.61	1.0	4.0	0.74
Zn	213.857	1.9	1.1	5.06	1.5	22.5	0.20
Pb	261.417	1.2	0.4	8.60	1.0	1.2	2.40
Cd	228.802	0.8	8.6	0.28	1.2	22.5	0.16
Te	238.579	1.6	0.4	4.86	1.1	2.1	1.60
Se	196.090	1.0	0.1	22.6	1.5	0.4	10.7
Sb	253.852	1.6	0.2	19.0	0.5	1.4	1.10
Bi	223.060	1.2	0.6	5.60	0.7	1.9	1.09

[a] Wavelengths correspond to values listed in the NIST Atomic Spectra Database;
[b] SBR is the Signal-to-Background ratio for 1 mg L^{-1} Cu, Pb, Te, Se, Sb and Bi and 0.1 mg L^{-1} Cd, Zn and Hg [b] LOD was calculated according to the SBR-RSDB approach [26, 27];

Table 3. Comparison of LODs for the Mo flat coil filament SSETV-μCCP-OES method with other ETV-based microanalytical systems

Element	SSETV-μCCP-OES (Mo flat coil)	ETV-DBD-OES (Mo coil) [24][a]	ETV-DBD-OES (W coil) [12][b]	ETV-DBD-OES (W coil) [14][c]	ETV-PD-OES[f] (Re coil) [30][d]	ETV-PD-OES[f] (W coil) [21][e]
Hg	0.20	0.40	-	-	-	-
Cu	0.74	7.94	-	-	1.5	15
Zn	0.17	1.89	24	-	20	5
Pb	2.40	8.95	-	7.7	20	8
Cd	0.16	0.65	0.8	-	20	0.08
Te	1.60	-	-	-	-	-
Se	10.7	-	-	-	-	-
Sb	1.10	-	-	-	-	41
Bi	1.09	-	-	-	-	40

[a] Sample volume: 3 μL, plasma power: 37 W;
[b] Sample volume: 10 μL, plasma power: 2 W;
[c] Sample volume: 20 μL, plasma power: 30 W;
[d] Sample volume: 3 μL, plasma power: 4 W;
[e] Sample volume: 10 μL, plasma power: 0.8–3.2 W;
[f] ETV-PD-OES – electrothermal vaporization point discharge optical emission spectrometry

A comparison between various analytical systems, including those based on optical emission spectrometry using microplasma sources, is challenging without considering the characteristics of the micro sample introduction device, the sample volume, and the operating conditions of the microplasma, particularly the power. Therefore, in miniaturized systems employing electrothermal evaporation, the emission signal is directly proportional to both the micro sample volume and the microplasma power at a given analyte concentration. Thus, the LODs for Hg, Cu, Zn, Pb, and Cd obtained using the SSETV-μCCP-OES experimental setup with the Mo flat coil filament were superior to those reported by Li et al. [24] using ETV-DBD-OES with a Mo coil, primarily due to the use of a 10 μL sample volume in our study, compared to only 3 μL in the DBD microplasma system. A similar trend was observed for Zn and Cd, compared to those reported using the ETV-DBD-OES system with a W filament. This enhancement is attributed to the higher microplasma power employed in our setup (15 W), in contrast to the 2 W used in the DBD microplasma configuration. Compared to the ETV-DBD-OES setup with a W filament, the achieved LOD for Pb using our experimental configuration was superior, despite using only half the micro-sample volume and a plasma power two times lower than those employed in the DBD microplasma system [14]. This is likely due to a lower spectral background of the capacitively coupled microplasma and an improved signal-to-background ratio. Compared to the experimental ETV-MPD-OES system with a Re filament [30], in which a volume of 3 μL sample and a microplasma power of 4 W was employed, our limits of detection for Cu, Pb, Zn, and Cd were also superior, as a result of the aforementioned considerations. In the case of the ETV-PD-OES system [21], which employed a W filament, a sample volume of 10 μL, and an operating power of up to 3.2 W, the limits of detection for Cu, Zn, Pb, Sb, and Bi were also superior to those obtained with our SSETV-μCCP-OES setup using the Mo flat coil filament. These findings highlight that the Mo flat coil filament, designed and fabricated in our laboratory, is a promising device for use in a miniaturized ETV configuration coupled with microplasma-based optical emission spectrometry for trace metal analysis. By using a faster heating rate, the LODs were substantially improved, and the method can be applied to food, environmental, and polymeric material samples subjected to acid digestion; however, further studies are needed to evaluate potential matrix effects caused by the presence of concomitant elements in the sample matrix.

CONCLUSIONS

A novel SSETV device based on innovative molybdenum flat coil filament was successfully used for microsample introduction in a capacitively coupled microplasma for the simultaneous multielemental determination of Cu, Zn, Pb, Cd, Hg, Se, Te, Sb, and Bi by optical emission spectrometry. The Mo flat coil filament allowed better limits of detection to those previously obtained by the same SSETV-μCCP-OES equipped with a Rh coil filament. This was attributed to a faster vaporization process and an improved signal-to-background ratio (SBR). Furthermore, the comparative data obtained using the SSETV-μCCP-OES setup with the Mo flat coil filament, in relation to other miniaturized microplasma-based analytical systems reported in the literature, confirmed its analytical capabilities required for multielement trace metals analysis in liquid microsamples.

EXPERIMENTAL SECTION

Reagents and solutions

Single element ICP standard solutions of Cu, Zn, Pb, Cd, Te, Se, Sb, Bi and Hg of 1000 mg L^{-1} in HNO_3, purchased from Merck (Darmstadt, Germany), were used for the preparation of 1 mg L^{-1} Cu, Pb, Te, Se, Sb and Bi and 0.1 mg L^{-1} Cd, Zn and Hg multielement-standard solution by serial dilution with 2% (v/v) HNO_3. Nitric acid 65% (m/m) for analysis (max 0.005 mg L^{-1} Hg) was purchased from Merck (Darmstadt, Germany). A solution of 5% (v/v) HNO_3 was used for decontamination of glassware by immersion overnight, followed by rinsing with ultrapure water (18 MΩ cm), obtained using a Milli-Q water purification system (Millipore, Bedford, USA).

Instrumentation

The μCCP-OES instrumentation was similar to that previously used, with the exception of the Rh coil filament, which was replaced by a small-sized electrothermal vaporization device based on Mo flat coil filament [17]. The SSETV-μCCP-OES setup used in this study consisted of the following components: (1) a home-made capacitively coupled microplasma (μCCP-OES) as excitation source (2); a miniaturized RF generator of 13.56 MHz (Technical University, Cluj-Napoca, Romania), operated at low power (15 W) and low Ar flow rate (150 mL min^{-1}); (3) a Maya2000 Pro CCD spectrometer with a spectral range of 165–309 nm and a Full Width at Half Maximum (FWHM) of 0.35 nm, Ocean Optics (Dunedin, USA); (4) a home-made Mo

flat coil filament as sample introduction system powered from a TENMA 72-13360 (TENMA Inc. China). The heating of the Mo filament was controlled by an application developed in Labview (National Instruments, USA) for sample drying at 80 °C for 180 s and vaporization at 1500 °C for 10 s. Simultaneously with the evaporation of a volume of 10 µL microsample, the transient emission spectrum was recorded over a period of 10 s with an integration time of 100 ms per episode for all elements. The Mo flat coil filament, the SSETV setup was incorporated in a 3D printed sample introduction system from polyacrylamide using the Creality K1 3D equipment (Shenzhen Creality 3D Technology Co., Ltd., China) (Figures 1 and 2). The 3D printing conditions were: 0.4 mm nozzle diameter, 230 °C nozzle temperature, 45 °C platform temperature, 8–15% sparse infill density, diamond infill pattern, 2 mm s^{-1} printing speed, 0–15% internal fill density of support material and diamond infill pattern of support material. The Mo flat coil filament was manufactured from a 0.13 mm thick Mo sheet, with a purity of 99.9% (JSflline Material Store, China), cut into a coil geometric form using a laser cutting equipment (Fiber laser MOPA 30w, China).

The Mo flat coil filament is installed and fixed on a PTFE piston with the aid of epoxy resin (Figure 2, (5)), using a set of two cables soldered to its two terminals and passed through the piston body in the middle for connection to the power supply. The piston support (2) includes a cover with a cutout for attaching the lever and couplings, and at the end of the piston support, the mount with the iris-type mechanism (1) is installed, which includes a shaft and a spring to guide the iris actuator slider (6). The lever (3) is attached to the rod and inserted through a channel of the iris-type mechanism. When the piston is moved, the lever is also engaged, which in turn moves the iris actuator slider, namely opening it during forward motion and closing it during retraction. This mechanism converts the horizontal movement of the piston into a vertical movement of the slider. The iris opening and closing zones are correlated with the slope on the lever, and the positioning of the lever on the piston determines the moment at which the iris begins to open or close, ensuring that the orifice remains open for the shortest possible time. Since it is crucial to have the slider in a position where the iris is closed when extracting the filament, and a gravitational solution was neither sufficient nor reliable, a spring (4) was chosen to act on the slider, ensuring it moves downward and keeps the iris closed. The heating of the filament was ensured by connecting the 4 wires to the power source, of which 2 served for voltage supply, while the other 2 were connected to the regulation loop (Sense) of the power supply. This ensured that the power source maintained the set voltage applied to the filament, eliminating voltage drops across the supply cables and the contacts at the power terminals.

Method figures of merit

The figures of merit of the SSETV-μCCP-OES method, were evaluated in terms of relative standard deviation of the background signal (RSDB,%), signal-to-background ratio (SBR), and limit of detection (LOD). Instrumental LODs were calculated using the SBR-RSDB approach [26, 27], previously developed by Boumans, according to equation (1)

$$\mathrm{LOD} = 3 \times 0.01 \times \mathrm{RSDB} \times \frac{c_0}{\mathrm{SBR}} \quad (1)$$

where, RSDB – is the relative standard deviation of the background signal from 10 episodic spectra (100 ms integration time) before micro sample introduction; c_0 – is the analyte concentration; and SBR – the signal-to-background ratio.

The analyte signal was obtained by time integration, using the signal generated by the pixel corresponding to the analytical line. The number of spectra in which the analytical signal appeared ranged from 15–64, depending on the temporal evaporation kinetics of the element.

ACKNOWLEDGMENTS

This work was supported by a grant of the Romanian Ministry of Research Innovation and Digitization through the Core Program within the National Research Development and Innovation Plan 2022–2027, carried out with the support of MCID, project no. PN 23 05. This work was also supported by a grant of the Romanian Ministry of Research, Innovation and Digitization, CNCS/CCCDI-UEFISCDI, contract nr. 15PED/2025, project number PN-IV-P7-7.1-PED-2024-0091, within PNCDI IV.

REFERENCES

1. T. Matusiak; K. Swiderski; J. Macioszczyk; P. Jamroz; P. Pohl; L. Golonka; *Sensor Rev.,* **2020**, *40*, 437–444.
2. D. A. Agrawal; R. Keçili; F. Ghorbani-Bidkorpeh; C. M. Hussain; *TrAC - Trends Anal. Chem.,* **2021**, *143*, 116383.
3. Y. Zhang; J. Liu; X. Mao; G. Chen; D. Tian; *TrAC - Trends Anal. Chem.,* **2021**, *144*, 116437.
4. A. Galuszka; Z. Migaszewski; J. Namieśnik; *TrAC - Trends Anal. Chem.,* **2013**, *50*, 78–84.
5. H. R. Badiei; C. Liu; V. Karanassios; *Microchem. J.,* **2013**, *108*, 131–136.

6. D. C. Gregoire; *Electrothermal vaporization sample introduction for inductively coupled plasma-mass spectrometry* in *Comprehensive Analytical Chemistry*, Elsevier, **2000**, *Vol. 34*, pp. 347–444.
7. Y.-I. Lee; J.-K. Kim; K.-H. Kim; Y.-J. Yoo; G.-H. Back; S.-C. Lee; *Microchem. J.,* **1998**, *60*, 231–241.
8. L. Huang; D. Beauchemin; *Electrothermal vaporization* in *Sample Introduction Systems in ICPMS and ICPOES*, ed. by D. Beauchemin, Elsevier, Amsterdam, **2020**, pp. 411–467.
9. M. Aramendía; M. Resano; F. Vanhaecke; *Anal. Chim. Acta.,* **2009**, *648*, 23–44.
10. M. Resano; F. Vanhaecke; M. T. C. de Loos-Vollebregt; *J. Anal. At. Spectrom.,* **2008**, *23*, 1450–1475.
11. G. C. Y. Chan; G. M. Hieftje; N. Omenetto; O. Axner; A. Bengtson, et al.; *Appl. Spectrosc.,* **2024**, *79*, 481–735.
12. X. Jiang; Y. Chen; C. Zheng; X. Hou; *Anal. Chem.,* **2014**, *86*, 5220–5224.
13. N. H. Bings; Z. Stefanka; *J. Anal. At. Spectrom.,* **2003**, *18*, 1088–1096.
14. H. Zheng; J. Ma; Z. Zhu; Z. Tang; S. Hu; *Talanta,* **2015**, *132*, 106–111.
15. Q. Jin; H. Zhang; W. Yang; Q. Jin; Y. Shi; *Talanta,* **1997**, *44*, 1605–1614.
16. T. Frentiu; E. Darvasi; S. Butaciu; M. Ponta; D. Petreus; R. Etz; M. Frentiu; *Microchem. J.,* **2015**, *121*, 192–198.
17. T. Frentiu; E. Darvasi; S. Butaciu; M. Ponta; D. Petreus; A. I. Mihaltan; M. Frentiu; *Talanta,* **2014**, *129*, 72–78.
18. P. J. Parsons; Y. Zhou; C. D. Palmer; K. M. Aldous; P. Brockman; *J. Anal. At. Spectrom.,* **2003**, *18*, 4–10.
19. G. Lan; X. Li; J. Yao; X. Yu; Q. Liu; C. Qiu; X. Mao; *Front. Nutr.,* **2023**, *10*, 1201801.
20. L. Qian; Z. Lei; X. Peng; G. Yang; Z. Wang; *Anal. Chim. Acta.,* **2021**, *1162*, 338495.
21. Y. Deng; J. Hu; M. Li; L. He; K. Li; X. Hou; X. Jiang; *Anal. Chim. Acta.,* **2021**, *1163*, 338502.
22. S. N. Hanna; K. Joseph; C. J. C. P.; B. T. and Jones; *Instrum. Sci. Technol.,* **2011**, *39*, 345–356.
23. A. C. Davis; C. P. Calloway; B. T. Jones; *Talanta,* **2007**, *71*, 1144–1149.
24. N. Li; Z. Wu; Y. Wang; J. Zhang; X. Zhang; H. Zhang; W. Wu; J. Gao; J. Jiang; *Anal. Chem.,* **2017**, *89*, 2205–2210.
25. J. A. Rust; G. L. Donati; M. T. Afonso; J. A. Nóbrega; B. T. Jones; *Spectrochim. Acta B.,* **2009**, *64*, 191–198.
26. P. W. J. M. Boumans; *Spectrochim. Acta B.,* **1991**, *46*, 431–445.
27. P. W. J. M. Boumans; J. C. Ivaldi; W. Slavin; *Spectrochim. Acta B.,* **1991**, *46*, 641–665.
28. S. B. Angyus; E. Levei; D. Petreus; R. Etz; E. Covaci; O. T. Moldovan; M. Ponta; E. Darvasi; T. Frentiu; *Molecules,* **2021**, *26*, 2642.
29. S. B. Angyus; M. Senila; T. Frentiu; M. Ponta; M. Frentiu; E. Covaci; *Talanta,* **2023**, *259*, 124551.
30. S. Weagant; V. Chen; V. Karanassios; *Anal. Bioanal. Chem.,* **2011**, *401*, 2865–2880.